Article

Numerical Simulation of Axial-Flow Pump Cavitation Based on Variable Frequency Speed Regulation

Jincheng Ye, Linwei Tan *, Weidong Shi *, Cheng Chen and Egbo Munachi Francis

School of Mechanical Engineering, Nantong University, Nantong 226019, China
* Correspondence: tanlinwei@ntu.edu.cn (L.T.); wdshi@ujs.edu.cn (W.S.)

Abstract: In order to investigate the influence of variable voltage and variable frequency (VVVF) regulation on the cavitation performance of the axial-flow pump, numerical simulation and experiments were used to analyze the cavitation performance of an axial-flow pump under different VVVF modes. The VVVF modes were uniform acceleration with constant acceleration, variable acceleration with increasing acceleration, variable acceleration with decreasing acceleration, and its corresponding deceleration scheme. Furthermore, a comprehensive performance test rig was built for the pump to carry out cavitation visualization tests which verified the accuracy of numerical simulation. For the uniform acceleration scheme with constant acceleration, the change of flow field inside the impeller was stable, the expansion rate of cavitation was slow, and the growth rate of the cavitation volume was the slowest. For the variable acceleration scheme with decreasing acceleration, the cavitation extended rapidly due to the large initial velocity. For the variable acceleration scheme with increasing acceleration, cavitation extension was the slowest. The growth rate of the cavity volume of the two variable acceleration schemes was faster than that of the uniform acceleration scheme, and the changing trend was consistent. This feature indicates that the impeller rotation speed has a significant impact on cavitation, and excessive rotation speed will rapidly extend the cavitation. By monitoring the influence of cavitation on pressure distribution under VVVF, it was shown that the three acceleration schemes all produce large pressure fluctuation. For the uniform acceleration scheme with constant acceleration, the fluctuation range of pressure was more balanced, and the pressure dropped slowly. For the acceleration scheme with higher acceleration, the pressure fluctuation amplitude increased in the late stage of acceleration and the pressure decline speed accelerated. For the acceleration scheme with decreasing acceleration, the pressure showed a downward trend with violent fluctuations in the early stage and gradually tended to be flat in the late stage.

Keywords: axial-flow pump; numerical simulation; variable voltage; variable frequency; cavitation performance

1. Introduction

In recent years, with the continuous development of intelligence, great achievements have been made in water conservancy informatization, and intelligent water conservancy and intelligent irrigation have been gradually integrated into our daily life [1,2]. The cavitation problem of the axial-flow pump under VVVF has become one of the most urgent problems to be solved for an intelligent pump. Axial-flow pumps have the characteristics of large flow, low head, and simple structure, and are widely used in irrigation, water conservancy engineering, urban industry, and other industries [3,4]. VVVF can make the pump station maintain the highest operating efficiency at any time, reduce energy loss, and improve energy-saving characteristics, and is an indispensable technology for pumps [5]. The axial-flow pump is more prone to cavitation than other types of pumps due to its characteristics of large flow and low head. Especially in the case of large flow deviating from the design condition, the blade back of the axial-flow pump has a wide range at low pressure and is prone to serious cavitation [6–9]. Long-term cavitation will

have a negative effect on the energy conversion of the impeller, leading to a decrease in the hydraulic performance of the pump unit [10]. It will also induce vibration and noise in the pump device and can even cause cavitation damage to the axial-flow pump's blades, which will seriously affect the operation safety of the pump station [11]. Research on the cavitation performance of axial-flow pumps based on variable frequency speed regulation is of great significance to improving the performance and reliability of the intelligent operation of the axial-flow pump. This research can greatly promote the further development of intelligent pumps and has great significance for boosting intelligent water conservancy and intelligent irrigation.

At present, there has been relatively mature research on VVVF and cavitation in axial-flow pumps. Fei, Z. et al. used PLC software to build a variable frequency constant pressure water supply control system which can realize real-time monitoring of the operating environment and achieve a good energy-saving effect [12,13]. Zmf A. used theory, programming calculation, and experimental research to study the variable speed scheme of the pump and found a variable frequency method that could improve the system efficiency and power-saving rate [14]. Dmitriev, A. designed an algorithm to maintain pressure value and optimize efficiency for the process of frequency conversion speed regulation [15]. Cimorelli, L. et al. successfully reduced energy consumption loss and operating cost by using variable speed drive technology [16]. In the research of cavitation, Li Lin-min. et al. used a very large eddy simulation approach to investigate the conditions from inception to sheet/cloud cavitation regimes for the flow field and the dynamic characteristics of transient cavitating flow [17–19]. Zhong, L. proposed a brand-new cavitation coefficient determination method by combining a camera and vibration sensor [20]. Xin, L. et al. used the FBM model to predict the cavitation performance of the axial-flow pump and pointed out that the prediction accuracy would be higher in the case of small flow [21,22]. Through the frequency conversion speed system, Peng, W. designed a method to judge through the VVVF system whether cavitation occurs in axial-flow pumps based on the head deviation converted from the actual head and similar theory [23]. However, there are few studies on the cavitation phenomenon in VVVF, which has certain blindness.

In this paper, numerical simulation and experimental analysis were used as the methods, three-dimensional turbulence numerical simulation was used as the primary research method, and CFX was used as a computing platform. Then, an axial-flow pump was be dealt with VVVF and the influence of cavitation on pump performance during VVVF was analyzed. Finally, the accuracy of the numerical simulation was verified by experimental analysis.

2. Pump Model, Griding and Boundary Conditions

2.1. Computational Model

In this study, the axial-flow pump of an agricultural irrigation pump station was taken as the prototype pump with a specific speed of 735. An impeller model pump with a diameter of 200 mm was obtained using the similarity theory conversion as the research object. The main model structure is shown in Figure 1. The main flow components included a front water inlet pipe, impeller, guide vane, guide vane support plate, elbow, and outlet pipe. Table 1 lists the basic design parameters.

Table 1. Main geometric parameters of the model pump.

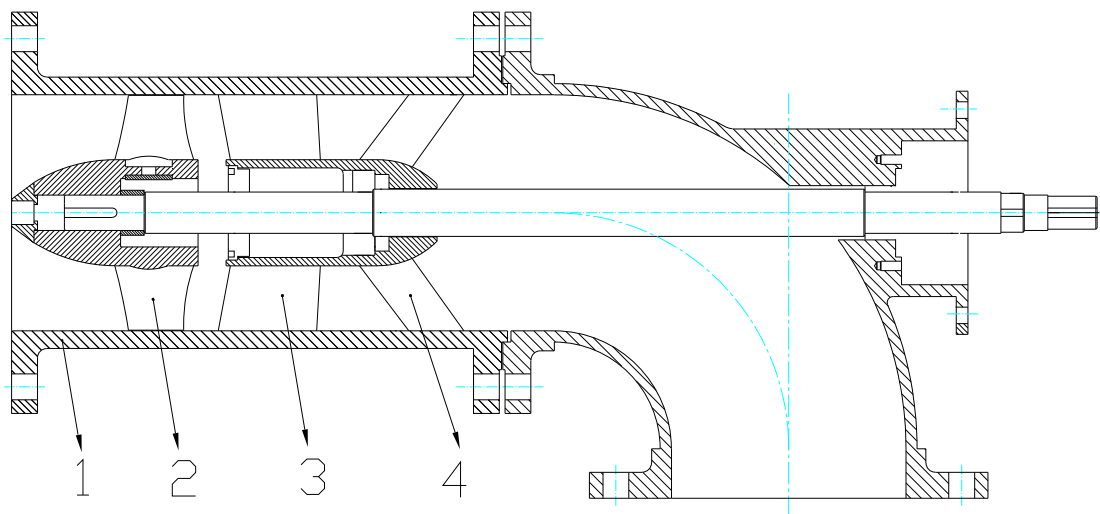| Main Parameters	Value
Flow (m^3/h)	365
Head (m)	3.02
Number of blades-Z_i	3
Number of guide blades-Z_s	7
Rated speed-n (r/min)	1450
Impeller inlet diameter-D_0 (mm)	200
Impeller outlet diameter-D_2 (mm)	250

Figure 1. Two-dimensional diagram of the axial-flow pump. **1.** Pipe **2.** Impeller **3.** Guide vane **4.** Guide vane support plate.

The 3D model of the axial flow pump was created by SolidWorks 2021. The main hydraulic components, such as the impeller and guide vane, are shown in Figure 2. In the process of model assembly, the gap between the impeller and the wall and the axial gap between the impeller and the guide blade were strictly controlled so that the structure conformed to the actual situation.
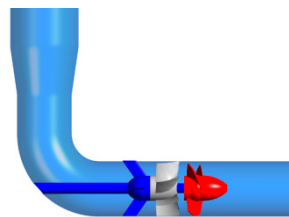

Figure 2. Three-dimensional structure diagram.

2.2. Grid Segmentation

SolidWorks was used to cut out the water body, and the water body model was saved according to the type of flow parts; the mesh was then divided pointwise. In order to improve the accuracy of numerical calculation and the simulation efficiency, the impeller area had a mixed grid. The inlet, outlet, and worm shell adopt the hexahedron structure mesh, which has good convergence. The number of grid nodes on each topology line was adjusted, the whole computing domain mesh was made uniform, and the grid was encrypted on the impeller region and interface. Figure 3 shows the position of the impeller, guide vane, and support plate of the axial-flow pump and the grid division of the water body.

To select the appropriate grid density, the grid should be tested for its independence. Taking the head as a reference point, when the head curve tends to be stable, it shows that the result converges. After analyzing a variety of grid quantities, a suitable scheme was selected. The grid size of each section is shown in Table 2.
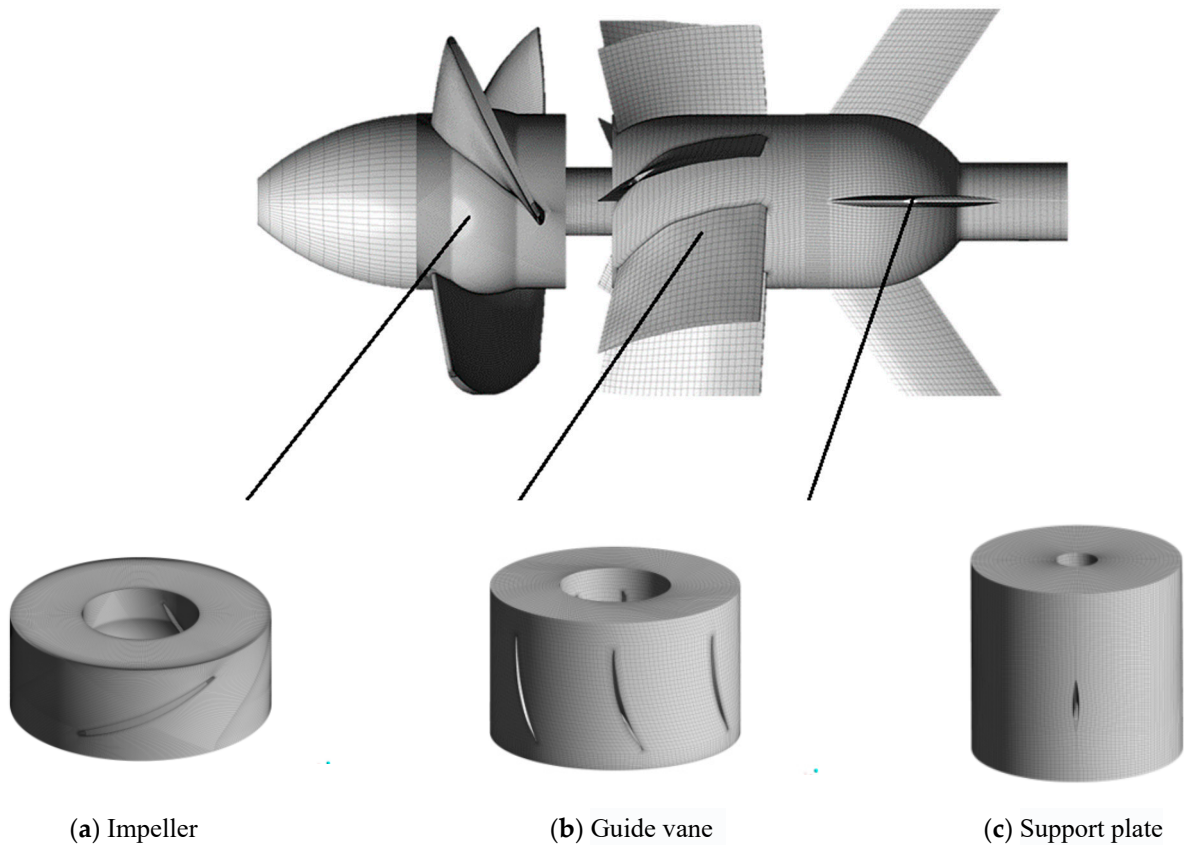
(**a**) Impeller   (**b**) Guide vane   (**c**) Support plate

Figure 3. Grid of main water body calculation domain.

Table 2. Local grid size.

Area	Part	Grid Form	Number of Grid	Number of Nodes
Inlet	Stationary domain	Structured grid	825,000	846,651
Impeller	Rotating domain	Structured grid	6,877,440	7,034,616
Guide vane	Stationary domain	Structured grid	1,355,585	1,415,904
Support plate	Stationary domain	Structured grid	179,520	190,400
Bend	Stationary domain	Structured grid	370,064	385,900
Outlet	Stationary domain	Structured grid	491,040	504,100

2.3. Numerical Methods

Based on the N–S equation and continuity equation, the flow characteristics of the shear layer pump are predicted by using an SST k-omega model. This method not only preserves the small-scale turbulence information near the wall but also accurately predicts the large-scale turbulence information in the separation area. The control equation is as follows:

$$\begin{cases} \frac{\partial(\rho k)}{\partial t} + \frac{\partial(\rho k u_i)}{\partial x_i} = \frac{\partial}{\partial x_j}\left[\left(\mu + \frac{\mu_t}{\sigma_{k3}}\right)\frac{\partial k}{\partial x_j}\right] + P_k - \beta^* \rho k \omega \\ \frac{\partial(\rho \omega)}{\partial t} + \frac{\partial(\rho \omega u_i)}{\partial x_i} = \frac{\partial}{\partial x_j}\left[\left(\mu + \frac{\mu_t}{\sigma_{\omega 3}}\right)\frac{\partial \omega}{\partial x_j}\right] + \alpha_3 \frac{\omega}{k} P_k - \beta_3 \rho \omega^2 + 2(1-F_1)\rho \frac{1}{\omega \sigma_{\omega 2}} \frac{\partial k}{\partial x_j}\frac{\partial \omega}{\partial x_j} \end{cases}$$

$$\mu_t = \rho \frac{a_1 k}{\max(a_1 \omega, SF_2)}, \quad P_k = \mu_t\left(\frac{\partial u_i}{\partial x_j} + \frac{\partial u_j}{\partial x_i}\right)\frac{\partial u_i}{\partial x_j} - \frac{2}{3}\frac{\partial u_k}{\partial x_k}\left(3\mu_t \frac{\partial u_k}{\partial x_k} + \rho k\right)$$

Within the equation: $\beta^* \rho k \omega$ is the dissipation term of the k equation; P_k is a turbulent synthesis term produced by viscous forces; F_1 and F_2 are two mixed functions of SST k-omega, and near the wall, F_1 and F_2 are 1. In the shear layer, F_1 and F_2 is 0.

2.4. Frontier Conditions

In this paper, numerical simulation was performed using ANSYS CFX. Water was chosen as a medium at 25 °C, the K-3 model was used as a computational model, smooth wall was used as a wall surface, the internal reference pressure was set to zero, the water vapor phase in the fluid material was added, and the vaporization pressure was set to 3540 Pa. Inlet and outlet conditions were adjusted according to the actual situation of the pump station. Convergence accuracy was set at 10^{-4}. The relevant parameters are shown in Table 3.

Table 3. Preprocessing condition setting.

Name of Hydraulic Component	Settings
Inlet	Total pressure: 50 kPa
Inlet pipe	Smooth wall surface
Impeller	Rotation speed: 1450 r/min Frozen rotor model
Guide vane	Smooth wall surface
Support plate	Smooth wall surface
Bend	Smooth wall surface
Outlet	Outlet flow: 365 m^3/h

Time step length is the key parameter of unsteady numerical calculation. Too small of a step length and too of a large step length will cost a great deal of computing resources. The time step must satisfy the Coolang number criterion, and the sampling theorem must be considered when monitoring the pressure pulse. This article set the time step length at 0.005 s.

2.5. Cavitation Model

In this paper, a Zwart cavitation model based on a simplified R-P equation was selected. The R-P equation, which can describe the process of cavitation and bursting, is the basic equation in cavitation dynamics. The equation assumes that there is no slip of relative velocity and no change of heat between the vapor–liquid phases when the medium is cavitated. The specific equations are:

$$R_B \frac{d^2 R_B}{dt^2} + \frac{3}{2}\left(\frac{dR_B}{dt}\right)^2 = \left(\frac{P_B - P}{\rho_l}\right) - \frac{4v_l}{R_B}\frac{dR_B}{dt} - \frac{2S}{\rho_l R_B}$$

R_B——Vacuum radius;
P_B——Vacuum surface pressure;
P——Infinity field pressure;
ρ_l——Liquid density;
v_l——Motion viscosity of liquids;
S——Liquid surface tension factor.

In order to solve the problem numerically, the relationship between bubble radius and media pressure can be deduced by ignoring the second order, viscous, and surface tension terms in the equation:

$$\frac{dR_B}{dt} = \sqrt{\frac{2}{3}\frac{P_B - P}{\rho_l}}$$

The change rate of the vacuole volume can be deduced by assuming that the vacuole volume is the ideal spheroid and replacing the vacuole radius with the vacuole volume:

$$\frac{dV_B}{dt} = \frac{d}{dt}\left(\frac{4}{3}\pi R_B^3\right) = 4\pi R_B^2 \sqrt{\frac{2}{3}\frac{P_B - P}{\rho_l}}$$

Based on the above formula, the change rate of cavitation mass can be derived:

$$\frac{\mathrm{d}m_B}{\mathrm{d}t} = \rho_v \frac{\mathrm{d}V_B}{\mathrm{d}t} = 4\pi R_B^2 \rho_v \sqrt{\frac{2}{3}\frac{P_B - P}{\rho_l}}$$

If the number of vacuoles per unit volume is N_B, the cavitation volume fraction formula is as follows:

$$\alpha_v = N_B V_B = \frac{4}{3}\pi R_B^3 N_B$$

The transfer of mass between vapors and liquids during cavitation is controlled by the transport equation of the vapour phase, which is as follows:

$$\frac{\partial}{\partial t}(\alpha_v \rho_v) + \nabla \bullet \left(\alpha_v \rho_v \vec{V_v}\right) = R_e - R_c$$

α_v——Vacuum volume fraction;

ρ_v——Vacuum density;

$\vec{V_v}$——The speed of the bubble;

R_e, R_c——Sources of mass transfer during vacuole growth and collapse.

The Zwart cavitation model chosen in this paper is compatible with almost all turbulence models. The four key parameters of the model are as follows: cavitation diameter, core volume fraction of cavitation, and evaporation and condensation coefficient.

The formula for the evaporation term R_e and condensation term R_c of this model is:

$$\begin{cases} R_e = F_{vap}\frac{3\alpha_{nuc}(1-\alpha_v)\rho_v}{R_B}\left[\frac{2}{3}\left(\frac{P_v - P}{\rho_l}\right)\right]^{\frac{1}{2}}(P \le P_v) \\ R_c = F_{cond}\frac{3\alpha_v\rho_v}{R_B}\left[\frac{2}{3}\left(\frac{P - P_v}{\rho_l}\right)\right]^{\frac{1}{2}}(P \ge P_v) \end{cases}$$

The empirical constant in the formula is as follows: evaporation factor $F_{vap} = 50$; condensation factor $F_{cond} = 0.01$; vapour volume fraction $\alpha_{nuc} = 5 \times 10^{-4}$; vacuum radius $R_B = 10^{-6}$ m.

2.6. VVVF Scheme

As, in the actual operation process and considering the safety condition, the pump speed of a single frequency change should not exceed 10%, the growth rate is too large to cause overload of the motor, friction loss, bearing loss, or packing loss; also, in the case of deceleration, too little speed and a rapid decrease in mechanical efficiency can lead to a decrease in pump efficiency, so that the average reduction in speed cannot exceed 30%. However, in the process of frequency conversion, it is difficult to observe the characteristic change of the pump. In order to highlight the comparison of pump performance under different rotational speeds, the increase in rotational speed was set at more than 50% of the rated speed, and the decrease in speed was set at half of the original rated speed.

This paper will use cel (CFX Expression Language) expression to simulate different forms of frequency conversion methods. The selected three-speed change forms and the corresponding acceleration scheme and deceleration scheme change forms are roughly the same. The speed change curve with time is shown in Figure 4.

Scheme one is the uniformly accelerated change in which acceleration is constant; in scheme two, the acceleration gradually increases, and the variation form is a quadratic curve with the opening direction upward. The third scheme is the variable speed change with decreasing acceleration, and the change form is also a quadratic curve with a downward opening direction. To study the influence of different frequency conversion modes on the flow field in the axial flow pump more accurately, after the completion of variable frequency speed regulation, the system ran stably again at the final speed of 0.5 s until the end of the numerical simulation after the completion of VVVF.
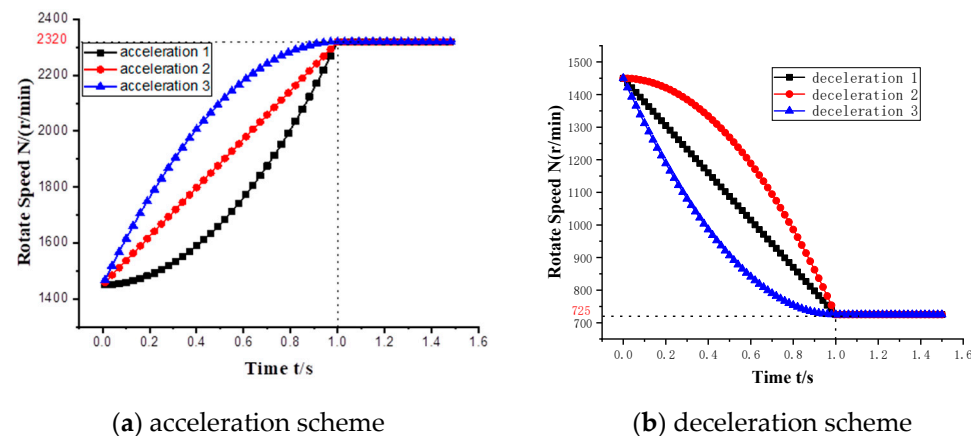
(**a**) acceleration scheme (**b**) deceleration scheme

Figure 4. Acceleration and deceleration scheme.

3. Experimental Model and Device

3.1. Experiment Apparatus

The experiment was completed at Nantong University School of Mechanical Engineering. The pipe diameter of the test bench was 150 mm, the inlet diameter of the pump was 200 mm, and the outlet diameter was 250 mm. The test bench was a closed circulation system which was mainly composed of a driving power device, model pump, pipeline pressurization system, circline, and pipeline flow control system. The schematics and pictures of the actual product are shown in Figure 5.
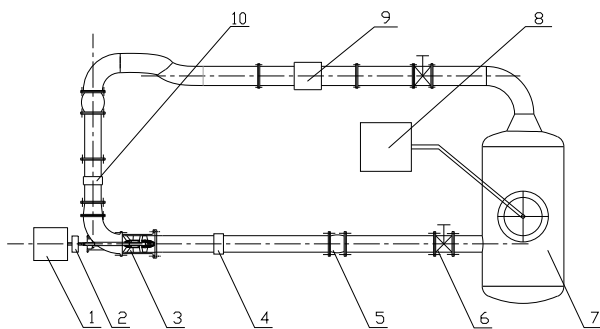
(**a**) (**b**)

Figure 5. Model pump experiment bench. (**a**) Schematic diagram of experiment bench. 1. Frequency conversion motor; 2. torque measuring instrument; 3. axial flow pump test section; 4. inlet pressure measuring section; 5. telescopic rubber hose; 6. watergate valves; 7. water tank; 8. vacuum pump; 9. electromagnetic flowmeter; 10. outlet pressure measuring section. (**b**) Picture of real products.

In this experiment, a 15 kW ABB three-phase asynchronous variable frequency motor was used. The relevant parameters were a synchronous rated speed of 1460 r/min and a frequency conversion range of 5–100 Hz. The inverter was used to control the motor operation, and the frequency conversion mode of the inverter was realized by computer programming.

The pump body section was made of transparent plexiglass shell, the impeller and guide vane parts were made of stainless steel and coated with a smooth black metal surface. Figure 6 shows the actual product. The basic parameters of the test pump were consistent with the previous model pump used for numerical simulation. From left to right in the figure are the support plate, guide vane, and impeller. The outer layer of the shell was transparent plexiglass, which made it easy to observe the formation and disappearance of cavitation in the flow field.
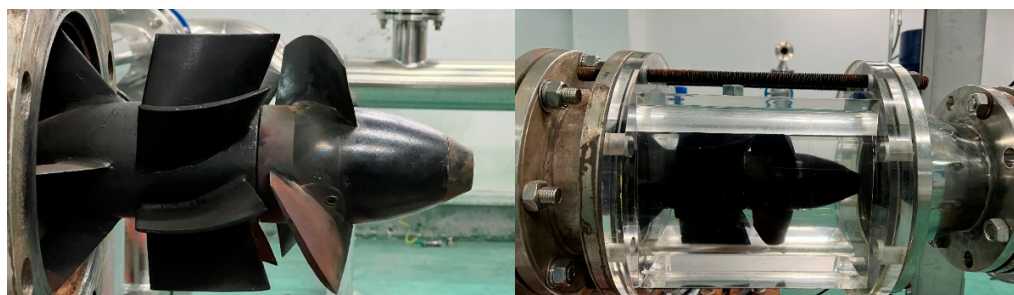
Figure 6. Impeller and guide vane.

3.2. Experiment Method

In order to verify the accuracy of the numerical simulation under VVVF, the cavitation visualization experiment was carried out on the axial flow pump. High speed cameras were used to capture the evolution of cavitation in the process of speed increase and compare the images of key time points with the numerical simulation results. Afterwards, the performance of the pump could be analyzed.

Due to the short time of VVVF and the limitations of the monitoring equipment, there was a significant delay in monitoring the transient head, and the real-time change of the transient head could not be accurately recognized. Therefore, this paper's cavitation visualization test will use a cavitation visualization experiment to explore the influence of cavitation performance on the impeller area of the axial-flow pump in the process of VVVF. In view of safety concerns, this experiment explored the cavitation development of the impeller area under a 1300–1600 r/min speed regulation interval, 1.0 Qopt corresponding flow rate, and 50 kPa inlet pressure. As shown in Figure 7, the camera was positioned in front of the test pump and captured an image every 1 ms. The pump pressure was reduced to 50 kPa before the start of the experiment, and the frequency converter accelerator was set up before each group of experiments. The total acceleration time was set to 1 s. At the beginning of the test, the camera was turned on and the speed control of the test pump was carried out through the inverter to record the cavitation. After one measurement was completed, the inverter was reset for cavitation determination in the second frequency conversion mode, and so on.
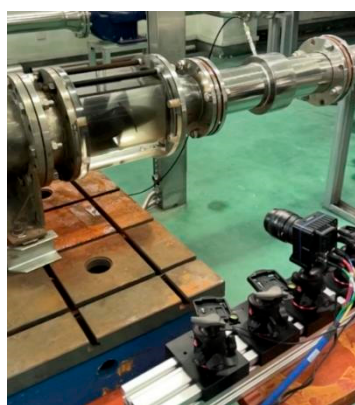

Figure 7. Cavitation visualization experiment.

4. Result and Discussion

4.1. Production of Cavitation in Axial Flow Pump

When the axial flow pump was running normally, the flow velocity on the back of the blade was higher and cavitation was most likely to occur. When the blade rotated to the left, cavitation mainly occurred at the inlet and outlet low pressure areas on the back of the blade. In addition, when the axial flow pump was running at a high flow rate, the

relative velocity at the inlet of the blade shifted outward, the inlet of the blade backflowed, and the low pressure cavitated. Under the condition of low velocity, the relative velocity of the leaf shifted in the opposite direction, and vortex backflow was generated in the back of the blade, which further exacerbated cavitation in the low-pressure area of the blade. In the process of speed regulation, especially acceleration regulation, the inlet pressure under the design conditions could not meet that of normal operation at high speed, the impeller speed was too high, so the suction surface pressure of the pump was further reduced, and the cavitation problem was more serious. In addition, the inlet condition of the pump was one of the important factors affecting cavitation of the pump. A bad water intake pipe produced vortex flow, increasing pump vibration.

4.2. The Evolution of Cavitation in the Process of VVVF

The axial-flow pump blade backside cavitation phenomenon is serious. This paper mainly analyzes the backside cavitation of the blade under different acceleration schemes. Figure 8 shows the distribution of the back blade surface cavitation volume fraction at different times. The rotation direction of the blade is counterclockwise.

It can be seen from the diagram that cavitation first occurs at the edge of the wheel at the inlet of the back of the blade and gradually extends to the root and outlet edge of the impeller as the speed of the impeller increases.

Under conditions of uniform acceleration, the cavitation extends more evenly until the blade surface appears completely cavitated after 0.5 s. Under variable acceleration with increasing acceleration, the time required for complete cavitation is the longest, and complete cavitation appears after 0.7 s. Under variable acceleration with decreasing acceleration, the cavitation extends rapidly, and the blade surface has been completely cavitation at about 0.2 s.

The simulation results show that the impeller rotation speed has a great influence on cavitation when the total inlet pressure is constant. Excessive initial acceleration will lead to a rapid deepening of cavitation.

According to the cloud diagram, cavitation mainly occurred at the tip of the blade. Then, under acceleration scheme 3, the cavitation volume distribution diagram with an inlet pressure of 50 kPa and blade height of 0.99 was mapped. Five time points from the whole speed change process were chosen for comparative analysis. As shown in Figure 9, there was a serious cavitation on the back surface of the blade, which gradually extended to the outlet as the rotational speed increased. When the acceleration would be completed at about 0.9 s, the cavitation at the outlet position of the blade was serious. In addition, the cavitation vortexes caused by the leakage of the impeller top also exist in the impeller passage. As the rotation speed increased, the cavitation vortex cluster grew larger and larger, eventually covering the entire back of the blade. The cavitation vortex cluster was roughly triangular in shape because of the uneven velocity of the tail of the blade.

The cel expression was edited for real-time monitoring of impeller cavitation volume fraction. As is shown in Figure 10, the horizontal axis represents the change in speed, the vertical axis represents the average cavitation volume of the impeller area, and the negative sign represents deceleration. Under the acceleration scheme, the cavitation volume fraction increased slowly before 1600 r/min. After 1600 r/min, the cavitation volume fraction rose in a straight line. At this time, most of the back of the impeller reached the cavitation critical state of the pump. Then, the cavitation volume fraction flattened after 1900 r/min.
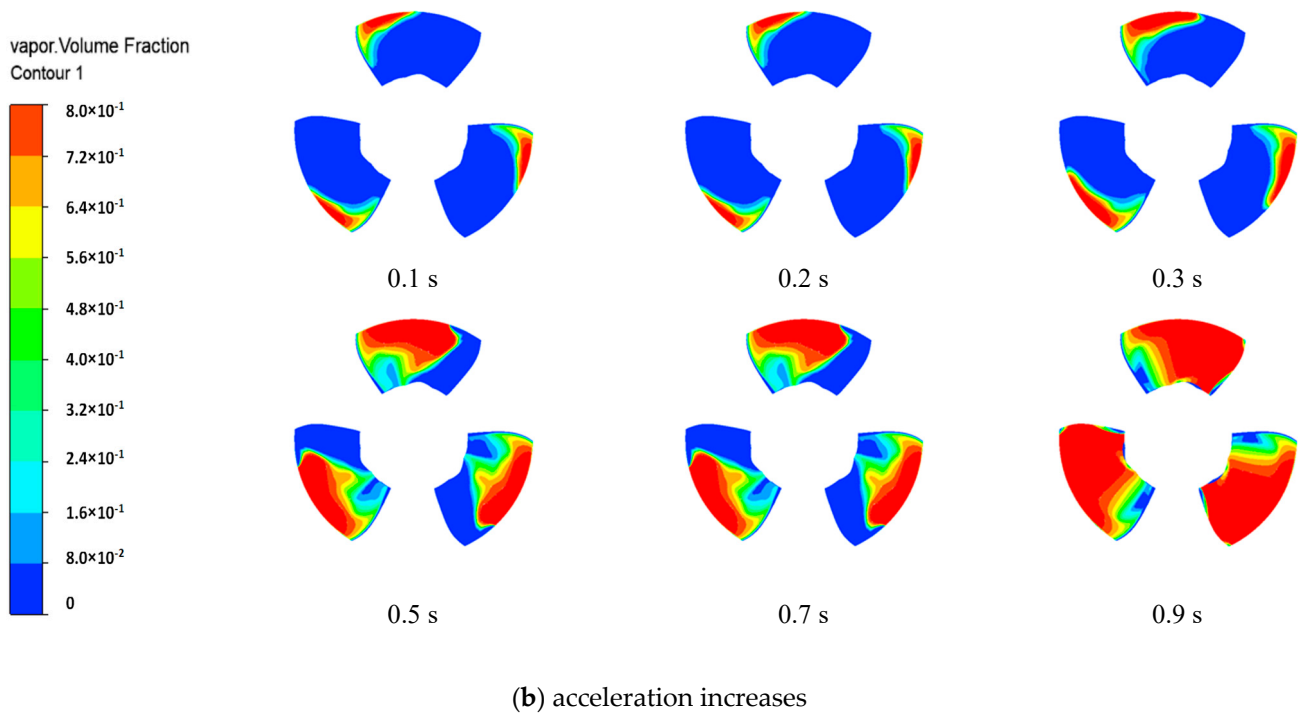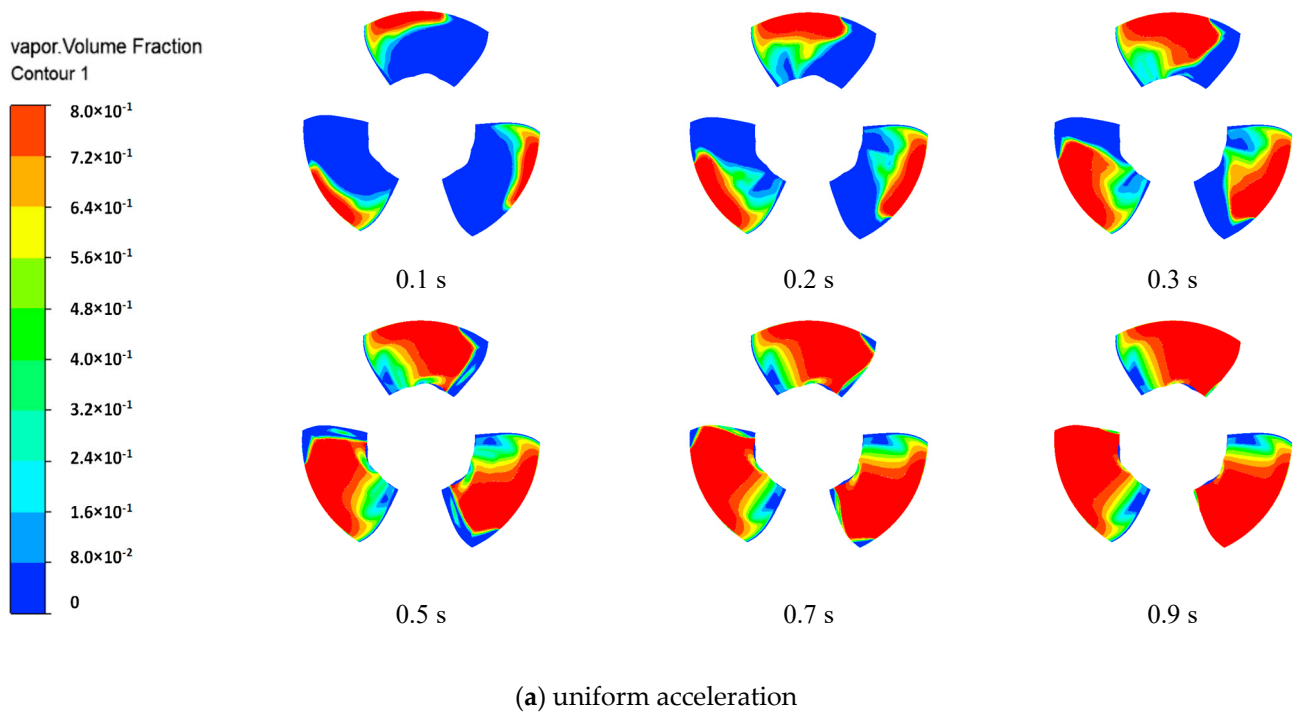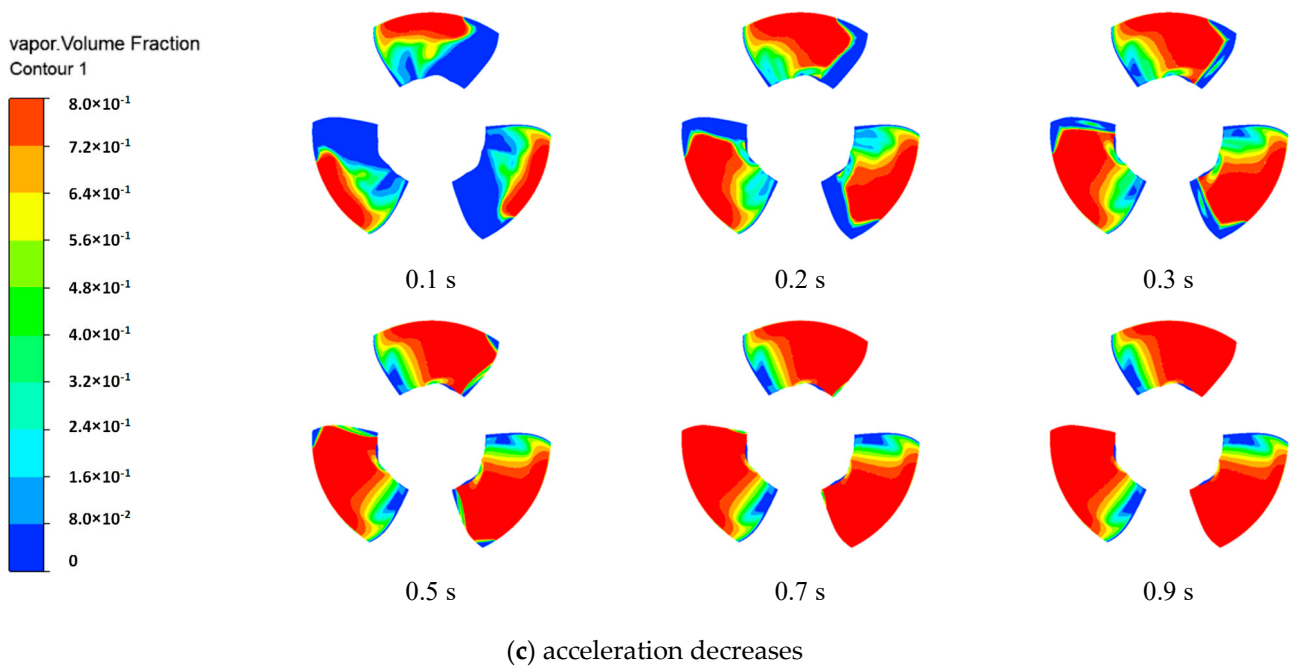
vapor.Volume Fraction
Contour 1

8.0×10^{-1}
7.2×10^{-1}
6.4×10^{-1}
5.6×10^{-1}
4.8×10^{-1}
4.0×10^{-1}
3.2×10^{-1}
2.4×10^{-1}
1.6×10^{-1}
8.0×10^{-2}
0

0.1 s 0.2 s 0.3 s

0.5 s 0.7 s 0.9 s

(**a**) uniform acceleration

vapor.Volume Fraction
Contour 1

8.0×10^{-1}
7.2×10^{-1}
6.4×10^{-1}
5.6×10^{-1}
4.8×10^{-1}
4.0×10^{-1}
3.2×10^{-1}
2.4×10^{-1}
1.6×10^{-1}
8.0×10^{-2}
0

0.1 s 0.2 s 0.3 s

0.5 s 0.7 s 0.9 s

(**b**) acceleration increases

Figure 8. *Cont.*

(**c**) acceleration decreases

Figure 8. Cloud diagram of cavitation volume fraction on the back of the blade.
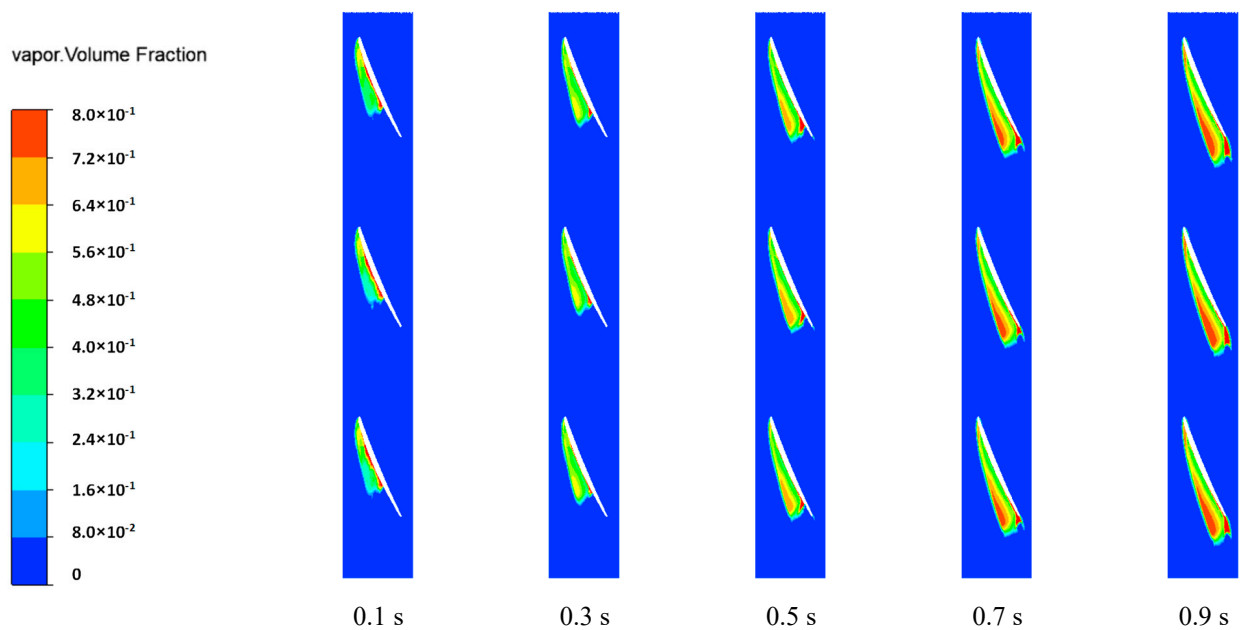
Figure 9. Expansion of cavitation cloud diagram on the blade surface.

4.3. Influence of Cavitation on Pressure Distribution

The appearance of cavitation affected the pressure change of the pump. To better explore the cavitation pressure distribution of each component, monitoring points were set inside flow components. For the impeller and the guide vane, four monitoring points were arranged from the edge of the inlet to the outlet, respectively. The flow of the support plate and bend was relatively stable, and the pressure distribution was relatively uniform, so only one monitoring point needed to be set there. The layout of the monitoring points is shown in Figure 11.

(**a**) acceleration　　　　　　　　　　(**b**) deceleration
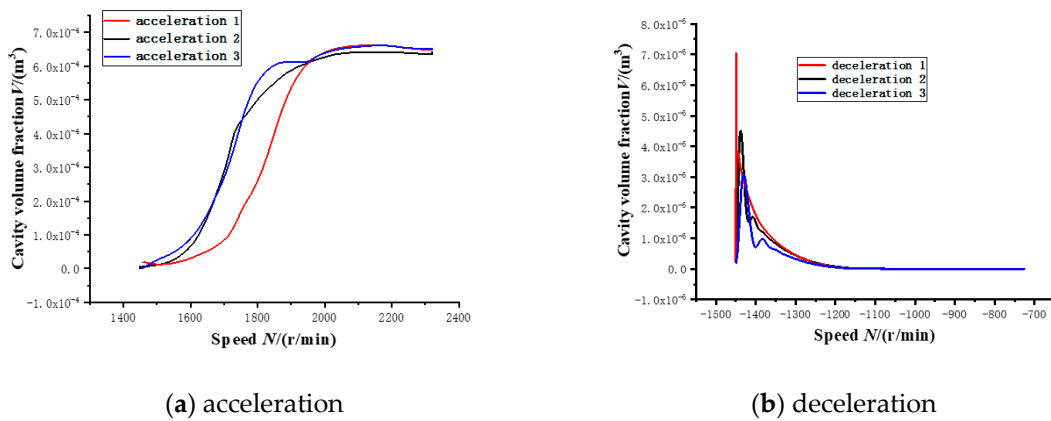
Figure 10. The average cavitation volume fraction in the impeller region.

(**a**) impeller　　　　　　　　　　　　(**b**) guide vane

(**c**) support plate　　　　　　　　　　(**d**) bend
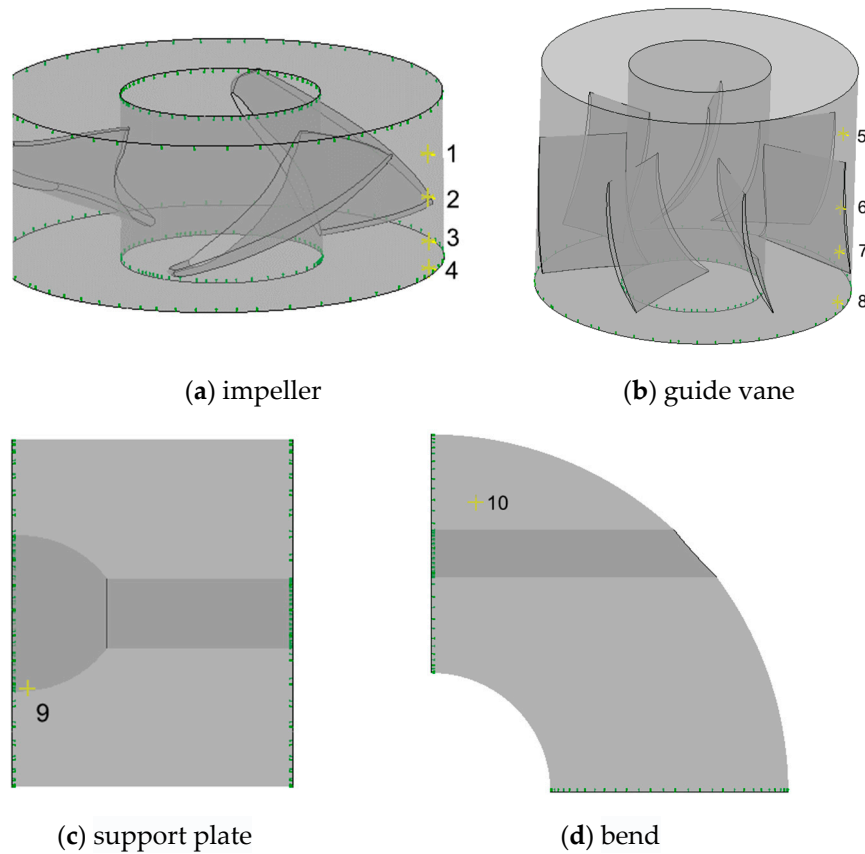
Figure 11. Layout of monitoring points.

The total pressure was kept at 50 kPa and then the pressure distribution of different flow components was monitored at different rotational speeds. The results are shown in Figures 12–15. The pressure distribution in the impeller area was complex, and the pressure fluctuation was obvious. The overall trend of change decreased over time, contrary to the absence of cavitation. This indicates that cavitation fundamentally changed the pump's original performance. Maximum pressure fluctuation occurred in the middle of the impeller. The maximum value was higher than that of other monitoring points under the same scheme, and the minimum was even close to 0 Pa, which was lower than the critical vaporization pressure for the cavitation phenomenon in the pump at that time. In addition, when observing the inlet and outlet monitoring points 1 and 4 in the impeller area, the pressure changes were also quite dramatic, especially at point 1—its pressure values were

basically between 4.0×10^4 Pa and 8.0×10^4 Pa, in which the fluctuation degree is close to the monitoring point in the middle. This phenomenon showed that cavitation affects the inlet and outlet water conditions, and that strong pressure fluctuation can easily lead to the vibration of the whole impeller area, which will greatly reduce the pump service life. Compared with the other three acceleration schemes, under the uniform acceleration scheme with constant acceleration, the cavitation degree in the pump deepened after 0.5 s, the maximum pressure inside impeller was near 10^5 Pa, and the pressure change degree intensified and began to drop. Under the acceleration scheme with increasing acceleration, the pump was completely cavitated and the pressure change degree increased by 0.7 s due to the increase of velocity, and the pump pressure fluctuated between 0 Pa and 8.0×10^4 Pa. Under the acceleration scheme with decreasing acceleration, the pressure had a downward trend after 0.2 s, and the velocity changed slowly after 0.8 s. The interference of the flow field was small, the pump pressure was basically stable below 6.0×10^4 Pa, and the pressure value tended to be stable. This situation indicates that cavitation does not affect the pressure distribution under VVVF.
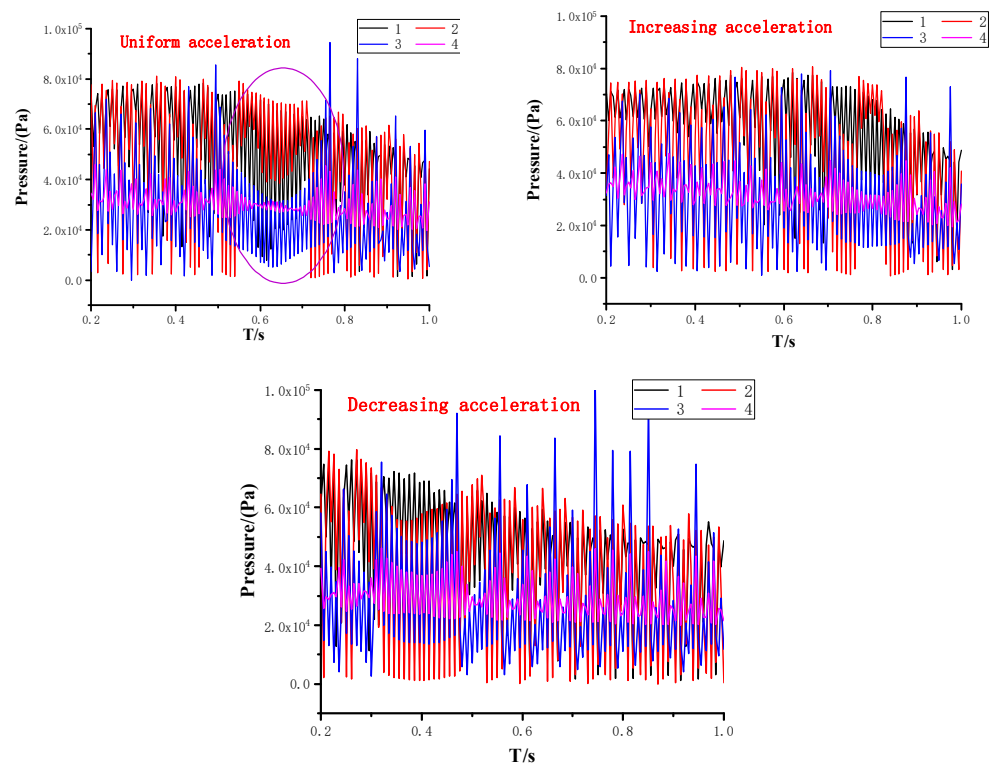

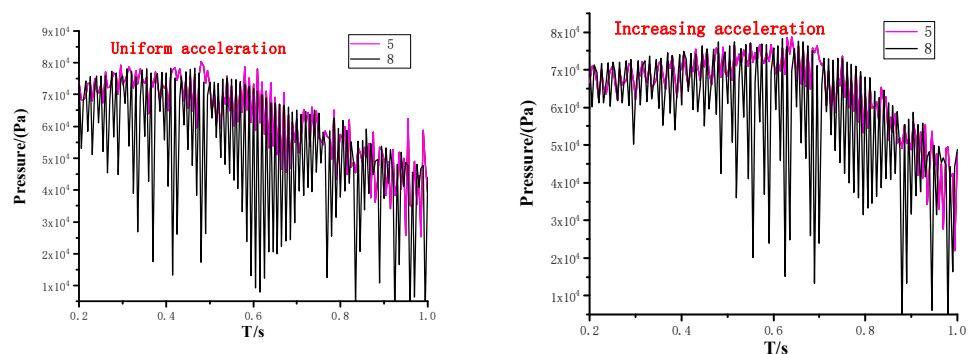**Figure 12.** Cavitation pressure distribution at impeller area.
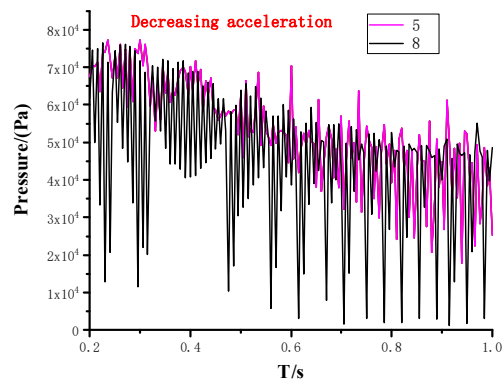

Figure 13. *Cont.*

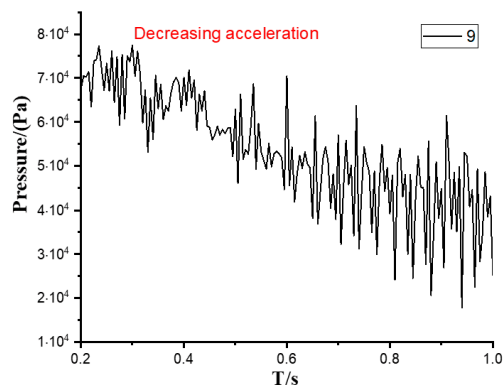**Figure 13.** Cavitation pressure distribution at guide vane.
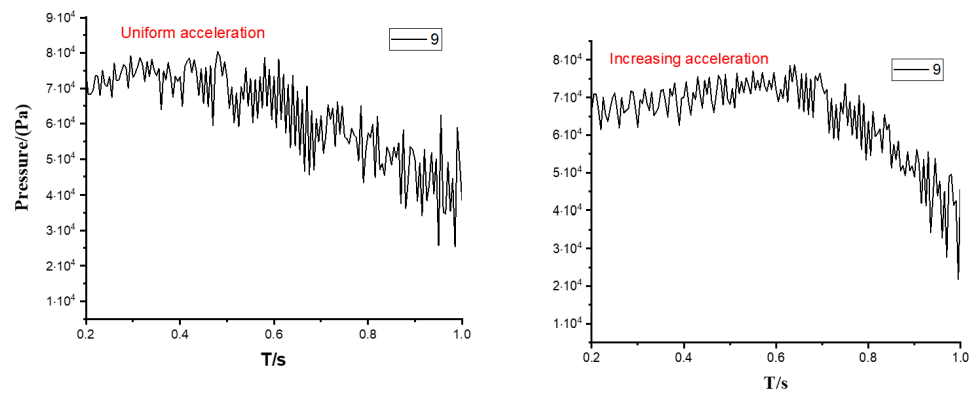

Figure 14. Cavitation pressure distribution at the support plate.
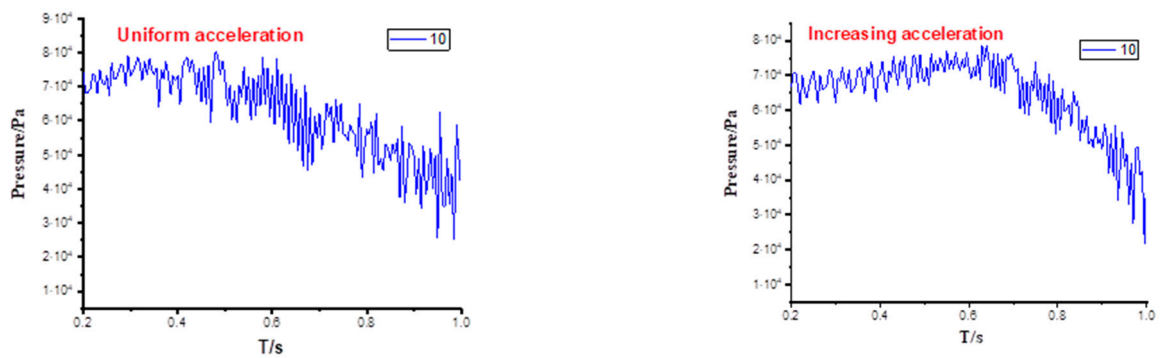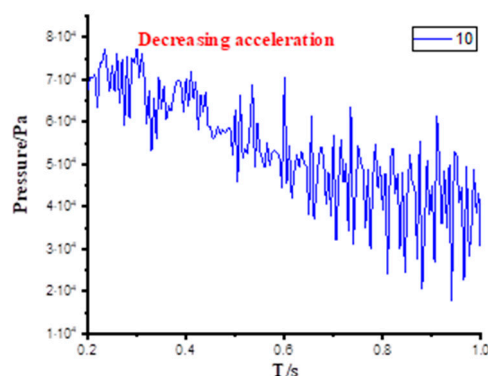

Figure 15. *Cont.*

Figure 15. Cavitation pressure distribution at the bend.

Observing the monitoring point in the inlet and outlet of the guide vane, the pressure fluctuation of the inlet position of the guide vane was obviously larger than that of the outlet position, which indicates that the cavitation had a direct influence on the inlet position of the guide vane; however, the pressure variation at the outlet position of the guide vane was consistent with that of the support plate and the bending pipe, which indicates that the cavitation had less effect on the flow path behind the guide vane.

We then compared the acceleration schemes according to the pressure distribution of the stationary parts. Under the uniform acceleration scheme with constant acceleration, the pressure fluctuation was not too great as a whole due to the velocity variation being more uniform, and the pressure began to decrease gradually after 0.5 s. Under the variable acceleration scheme with increasing acceleration, the pressure decreased rapidly as the acceleration increased and the velocity increased. Under the variable velocity scheme with decreasing acceleration, the initial acceleration value was larger, and the velocity variation was more obvious, so the pressure fluctuation was larger. However, when the acceleration gradually returned to zero, the velocity variation was no longer obvious. The pressure in the pump was almost constant under the influence of velocity, and the pressure distribution was almost cyclical. This phenomenon shows that acceleration has an obvious influence on the cavitation of stationary parts.

In conclusion, cavitation will affect the operating environment of the pump, the pressure fluctuation is large, and the variation is messy. The operating performance of the pump changes significantly with the generation and development of cavitation. As cavitation intensifies, the pressure drops sharply. Therefore, from the point of view of pressure distribution, cavitation greatly affects the pump's efficient operation, especially in the acceleration process, and cavitation development is extremely fast. If there is no effective means of control, VVVF will produce a counterproductive effect.

4.4. Experiment Results

The frequency conversion scheme mentioned above was used to obtain the pictures of the cavitation of the axial flow pump at speeds of 1450–1600 r/min. Six time points were then selected for comparison. As shown in Figures 16–18, at rated speed, the blade rotation speed was stable, streamline distribution was even, and cavitation was not obvious. Compared to the results of numerical simulation of the frequency conversion speed regulation, only a few cavitation particles appeared in the pump at the beginning of the acceleration, mainly at the tip position at the back of the blade, and the interval from generation to collapse was very short, with strong transient characteristics. With the increase of velocity, the blade cavitation group expanded to the exit gradually, forming a linear cavitation group. When the rotational speed increased further, the linear cavitation group gradually developed a gap between blades and blocked part of the impeller flow passage. The cavitation group moved with the flow to the guide vane, forming slight cavitation, which then covered the whole impeller flow channel upon hitting the guide vane. This conclusion is

consistent with the evolution of cavitation in numerical simulations. At this time, the pump body began to visibly vibrate, accompanied by the distinct sound of cavitation rupture. This phenomenon indicates that the cavitation in the pump at this time had been very serious, and the pump performance began to decline. In the later stage of acceleration, a relatively stable triangular cavitation group was formed on the blade suction surface. At this time, the head value began to decline, indicating that the influence of cavitation had exceeded the performance influence brought by increasing the speed.
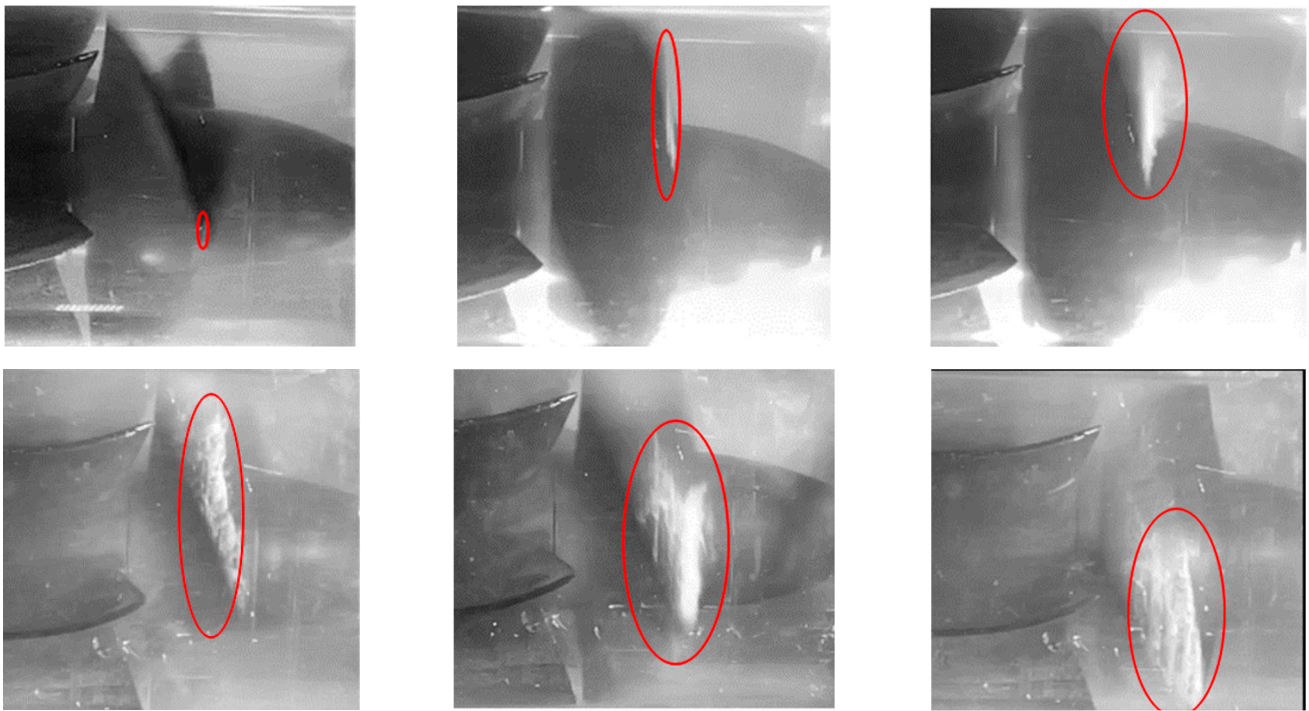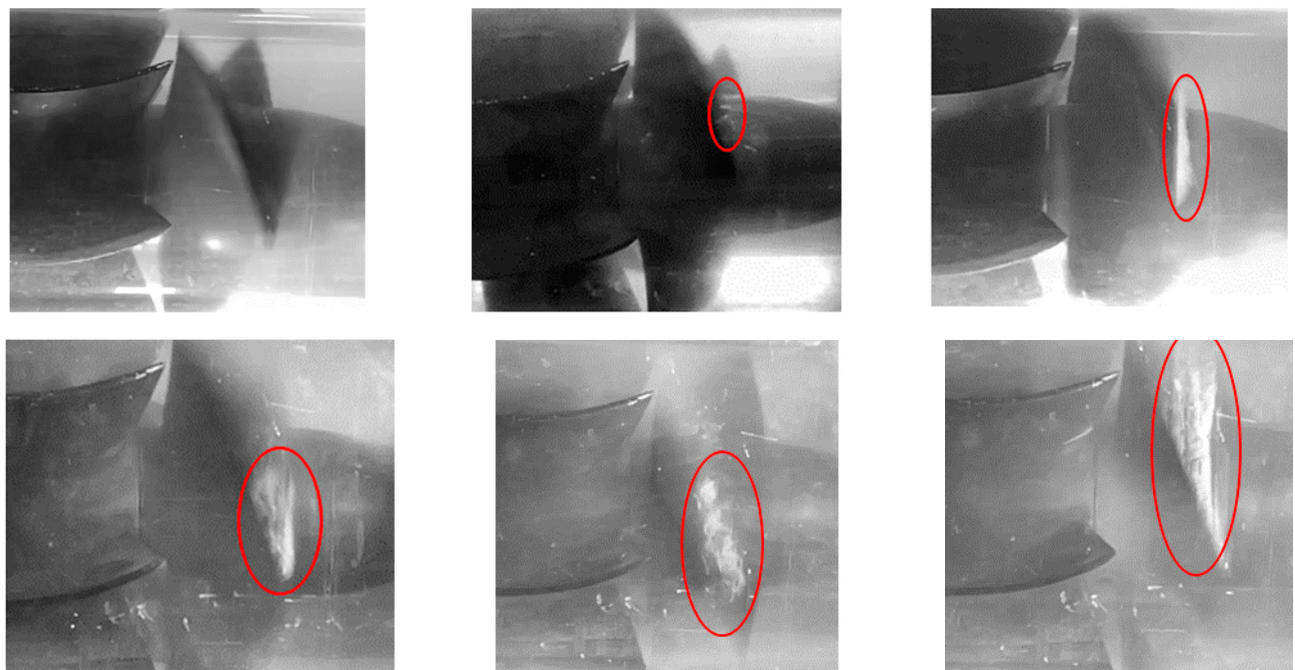

Figure 16. Acceleration scheme 1.

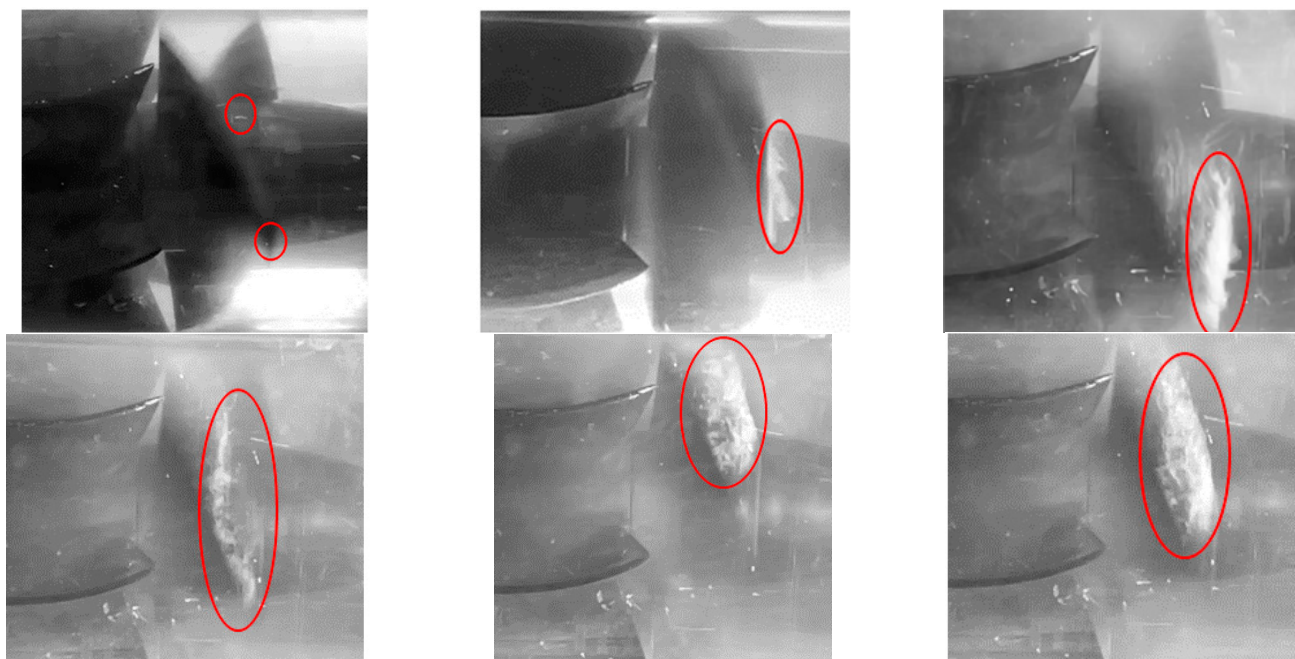**Figure 17.** Acceleration scheme 2.

Figure 18. Acceleration scheme 3.

　　Compared with the cavitation evolution process at different rotational speeds, the cavitation development speed under uniform acceleration scheme 1 is the most balanced, and a stable triangular cavitation cluster formed in the latter stage of acceleration. Acceleration scheme 2 has the slowest cavitation development speed—the cavitation is formed later, and the overall flow in the pump is more stable than other schemes. Under accelerated scheme 3, the cavitation mass develops the fastest, and it takes a very short time to spread to the whole flow channel from the beginning of cavitation. After 150 times of slow-down processing, it was found that by the time the impeller was rotated about 5 times, the impeller flow channel was already filled with a large number of cavitation groups, and the entire circulation pipeline also experienced slight vibration. This result shows that not only the change in speed but also the change in acceleration has a huge effect on the development of cavitation. Steady acceleration can promote the smooth development of pump cavitation. High-efficiency variable speed schemes can promote high-efficiency change of pump speed, but under the influence of cavitation performance, it will have a substantial influence on pump stability, which is consistent with the numerical simulation results. In practice, the pump should be kept running without cavitation as long as possible, especially in the acceleration process; when the pump work surface and back pressure gradient are large, slight cavitation can easily lead to vibration of the whole pump. Therefore, sufficient inlet pressure should be applied before VVVF to avoid cavitation.

　　The cavitation visualization experiment shows that cavitation occurs at the inlet position of the leaf tip on the back of the blade and extends to the flow path between the blade outlet and the blade as the speed increases. During the acceleration period, a stable, large triangular bubble is formed on the surface of the blade, and the pump unit vibrates violently. During the acceleration process, the cavitation performance of the test pump is controlled by speed and acceleration. The cavitation degree of the test pump under uniform acceleration increases slowly with time, while the cavitation of the test pump under constant acceleration changes dramatically. However, no matter which frequency conversion method is used, the cavitation phenomenon will occur after the acceleration, which will affect the performance of the pump. For a pump that needs frequency conversion for a long time, the inlet pressure should be increased as much as possible to restrain cavitation.

5. Conclusions

Based on a method combining numerical simulations and experiments, this paper studied the evolution of the cavitation of an axial-flow pump and the influence of cavitation on pressure under VVVF, and finally drew the following conclusions:

(1) The main area of cavitation is in the impeller region. The impeller rotation speed has a significant effect on cavitation. Excessive rotation speed will make cavitation extend rapidly. Under the frequency conversion scheme with reduced acceleration, it takes only 0.2 s for the impeller surface to completely cavitate.

(2) The growth rate of cavitation mainly depends upon the stability of velocity. In the case of constant acceleration, the growth rate of cavitation is the slowest. However, in the two-variable acceleration schemes, the growth rate of cavitation accelerates, and the change trend is the same.

(3) The pressure distribution in the pump will be seriously affected by cavitation. All three acceleration schemes generate large pressure fluctuation. Under the uniform acceleration scheme with constant acceleration, the fluctuation range of the pressure is more balanced, and the pressure drop is slow. Under the acceleration scheme with increasing acceleration, the pressure fluctuation amplitude increases, and the pressure decline velocity accelerates. Under the acceleration scheme with decreasing acceleration, the pressure in the early stage shows a downward trend with violent fluctuations and gradually tends to be flat in the later stage.

(4) Compared with the three VVVF schemes, the variable acceleration scheme with decreasing acceleration should be avoided as far as possible in order to reduce the influence of cavitation.

References

1. Jiang, Y.; Ye, Y.; Wang, H. Smart watershed and its application prospect. *Syst. Eng. Theory Pract.* **2011**, *06*, 1174–1181.
2. Wang, C.; An, G.; Yuan, C. Smart water development and key technology research. *Henan Water Conserv. S.—N. Water Transf.* **2015**, *14*, 98–100.
3. Ding, C. *Centrifugal Pump and Axial Flow Pump*; Machine Press: Beijing, China, 1981.
4. He, J.; Zhang, Y. Current situation and development of axial flow pump. *Water Pump Technol.* **1998**, *06*, 29–33.
5. Liu, X.; Su, Q.; Wu, L.; Yang, X. The small pump station is reformed to save electricity and increase income. *Nantong Daily* **2009**, *6*, A01.
6. Liang, W.; Ai, G.; Dong, W.; Wu, Z.; Zhu, J.; Liu, Y. Effect of cavitation on rotating solid coupling characteristics of axial flow pump blade. *Large Mot. Technol.* **2021**, *5*, 92–98.
7. Liang, W.; Hou, C.; Dong, W.; Wei, Q.; Wu, Z. Numerical analysis of cavitation characteristics of horizontal axial flow pump. *J. Drain. Irrig. Mach. Eng.* **2020**, *38*, 764–769.
8. Wang, J.; Pan, X.; Li, L. Cavitation of axial flow pump. *J. Drain. Irrig. Mach. Eng.* **2020**, *38*, 764–769.
9. Gao, Y.; Hou, Y.; Yang, Z.; Zhang, T. Static stress characteristics of axial-flow pump impeller under cavitation condition. *Agric. Eng.* **2018**, *8*, 84–90.

10. Wu, C.; Tang, F.; Yang, F.; Xie, C.; Sun, D. Effect of cavitation on energy conversion characteristics of impeller of axial flow pump. *Adv. Water Resour. Hydropower Sci. Technol.* **2019**, *39*, 49–74.

11. Fu, S.; Yuan, Z.; Kan, K.; Chen, H.; Han, X.; Liang, X.; Liu, H.; Tian, X. Numerical simulation and experimental study of transient characteristics in an axial flow pump during start-up. *Renew. Energy* **2020**, *119*, 1879–1887.

12. Zhao, Y.; Chen, Q. Application of PLC and frequency control technology in the constant pressure water supply of pump station. *Ind. Instrum. Autom. Equip.* **2004**, *15*, 56–65.

13. Hu, C.; Sang, R. PLC is used to realize variable frequency constant pressure water supply control system of pump station. *Drain. Irrig. Mach.* **2005**, *13*, 42–45.

14. Feng, Z.M.; Guo, C.; Zhang, D.; Cui, W.; Tan, C.; Xu, X.; Zhang, Y. Variable speed drive optimization model and analysis of the comprehensive performance of beam pumping unit. *J. Pet. Sci. Eng.* **2020**, *191*, 107155. [CrossRef]

15. Dmitriev, A.; Gerasimov, V. To the issue of energy efficiency of using frequency-controlled centrifugal pump units. *Matec Web Conf.* **2018**, *170*, 03017. [CrossRef]

16. Cimorelli, L.; Covelli, C.; Molino, B.; Pianese, D. Optimal Regulation of Pumping Station in Water Distribution Networks Using Constant and Variable Speed Pumps: A Technical and Economical Comparison. *Energies* **2020**, *13*, 2530. [CrossRef]

17. Li, L.-M.; Wang, Z.-D.; Li, X.-J.; Wang, Y.-P.; Zhu, Z.-C. Very Large Eddy Simulation of Cavitation from Inception to Sheet/Cloud Regimes by A Multiscale Model. *China Ocean. Eng.* **2021**, *35*, 361–371. [CrossRef]

18. Li, X.; Liu, Y.; Zhu, Z.; Lin, P.; Li, L. Boundary vorticity analysis and shedding dynamics of transient cavitation flow around a twisted hydrofoil. *J. Fluids Eng.* **2020**, *143*, 1–18. [CrossRef]

19. Liu, Y.; Li, X.; Wang, W.; Li, L.; Huo, Y. Numerical investigation on the evolution of forces and energy features in thermo-sensitive cavitating flow. *Eur. J. Mech.—B/Fluids* **2020**, *84*, 233–249. [CrossRef]

20. Li, Z. *Study on Cavitation Flow in Axial Flow Pump*; Jiangsu University: Zhenjiang, China, 2011.

21. Lv, X.; Zhen, Y.; Zhang, D.; Yu, A. CFD analysis of cavitation flow characteristics of axial-flow pump based on FBM model. *S.—N. Water Divers. Water Sci. Technol.* **2020**, *18*, 150–165.

22. Fu, Y.; Yuan, J.; Yuan, S.; Pace, G.; D'Agostino, L.; Huang, P.; Li, X. Numerical and experimental analysis of flow phenomena in a centrifugal pump operating under low flow rates. *J. Fluids Eng.* **2015**, *137*, 011102. [CrossRef]

23. Wu, Y. Method for measuring cavitation performance of axial-flow pump by frequency conversion. *Chem. Manag.* **2021**, *17*, 139–141.